Universiteit Leiden
The Netherlands

Numerical studies of the interstellar medium on galactic scales

Pelupessy, F.I.

Citation

Pelupessy, F. I. (2005, March 16). *Numerical studies of the interstellar medium on galactic scales*. Retrieved from https://hdl.handle.net/1887/619

Version:	Not Applicable (or Unknown)
License:	Leiden University Non-exclusive license
Downloaded from:	https://hdl.handle.net/1887/619

Note: To cite this publication please use the final published version (if applicable).

Chapter 5

Small star forming galaxies: the role of gas and halo parameters

Abstract

In this chapter we examine whether the observed structural differences between blue compact dwarfs (BCDs) and dwarf Irregular (dIrr) galaxies can explain the differences in star formation patterns for the two classes of dwarf galaxies. We concentrate on the role of the gas distribution and the central density of the dark halo, running N-body/smoothed particle hydrodynamics (SPH) simulations for galaxy models with different parameters. The simulations include a full model for the interstellar medium (ISM), star formation and feedback, and thus our simulations test for the first time the relation between BCD and dIrr galaxies in the context of a self-consistent model of a star forming galaxy. We find that our models show a variety of star formation patterns. High central gas surface densities show high star formation rates, while the presence of a high central halo density will produce a central starburst. Comparing our simulations with observations we conclude that both high central gas surface and a high central halo density are necessary for a system to exhibit BCD features.

5.1 Introduction

Compared with normal dwarf irregular (dIrr) galaxies, blue compact dwarfs (BCDs) have more centrally concentrated HI distributions and higher central halo densities, resulting in more steeply rising rotation curves (Meurer et al. 1998, van Zee et al. 2001). The classification of a galaxy as a BCD, which is made on the basis of the scale length of the light distribution, UBV colours and the presence of emission lines (Thuan & Martin 1981), implies that it undergoes an intense central burst of star formation, not sustainable over cosmological timescales. The gas consumption times of BCDs are in the order of about a Gyr (Thuan & Martin 1981, van Zee et al. 1998, Hunter & Elmegreen 2004). This, coupled to their low metallicity has been put forward as an argument for BCDs to be young systems experiencing their first starbursts. This notion has been discredited by the detection of aged stellar populations in BCDs (Papaderos et al. 1996, and references therein). Some systems may be truly young systems (e.g. Izotov & Thuan 2004), but these do not seem to be typical. While dIrr have widely varying properties, star formation in these systems is generally more spread throughout the disk and the rates of star formation are lower than for BCDs, with gas consumption timescales in the order of tens of Gyr (van Zee 2001). The ages of stars, as indicated by their colours are consistent with a more or less constant star formation history (SFH) on timescales of the order of 10 Gyr.

The differences in star formation properties between BCDs and dIrrs can be understood in general terms as resulting from the observed differences in halo and gas structure (see also the discussion in van Zee et al. 2001). The dependence of the star formation rate (SFR) on the gas surface density (Σ_{g}) can be fitted for a wide range of environments by the *Schmidt Law:* $\mathrm{SFR} \propto \Sigma_{\mathrm{g}}^{1.5}$ (Schmidt 1959, Kennicutt 1989), and thus more intense star formation is expected for systems with a higher central gas surface density. The steeply rising rotation curve, on the other hand, will stabilise BCDs against star formation, perhaps allowing for a larger supply of fuel to accrete, which enables a more intense starburst when star formation does start (van Zee et al. 1998).

However, these qualitative explanations should be tested in the context of a self consistent description of the star forming ISM. Clearly the complexities of the processes of star formation and feedback from young stars mean that the resulting system properties may not follow straightforwardly from empirical relations or plausibility arguments. For example, the instability criteria such as those based on the Toomre Q have been shown to be of limited value in predicting the amount and location of star formation in dwarf galaxies (Hunter et al. 1998). Also, the above argument does not answer the question what BCDs will look like after the current starburst, and which systems are candidates to be classified as quiescent BCDs, nor does it say anything about the extent to which ordinary dIrr can experience BCD phases.

Thus, numerical simulation of these systems with a code that includes the relevant physics of star formation and feedback, such as the code we have employed in Chapter 4, may be a useful tool to investigate star formation in these systems. Furthermore, a good “laboratory” model for star forming dwarf galaxies could be used for more detailed examinations of the evolutionary links between dIrr, BCD and dwarf Ellipticals (dE). Ultimately, one may be able to predict (or derive) from numerical simulations the star formation properties of a galaxy from the mass and angular momentum distribution and determine whether the mode of star formation could change over time, and thus obtain a theoretical framework linking the different species of dwarf galaxies.

For numerical modelling of galaxies one always encounters poorly constrained free parameters that arise because of the fact that processes, such as star formation and feedback are not fully represented. Matching between large surveys of dwarf galaxies and theoretical models would help to constrain these free parameters. This would also give information about the underlying distribution of cosmological initial conditions from which the current population of dwarf galaxies is formed. This is difficult to obtain because information about the primordial density spectrum on these scales is heavily convoluted with the effects of star formation and gas physics.

In this study we will examine dwarf galaxy evolution using N-body/SPH simulations. We will limit ourselves to a simple numerical experiment: what happens if we confront the observed gas and dark matter distributions with a numerical code that includes a realistic description of the ISM, star formation and feedback? The goal of this study is to examine whether the differences between the distribution of dark matter and gas found for dIrr and BCD are enough to explain the differences in star formation properties. Our numerical approach complements the large body of literature devoted to observational studies on this subject. Amongst the questions that we will try to answer are: do the simulated systems look similar to observed dwarf systems? How do the simulated systems evolve in time? Can BCD types and dIrr types morph into another? In Section 5.2 will first give a short description of the simulation method. We will discuss the range of our parameter study in Section 5.3, where we will also describe the initial conditions. In Sections 5.4 and 5.5 we present the results of our simulations and the observational characteristics that the simulated systems would present. Section 5.6 concludes with a discussion of the implications of our models for the classification of small star forming galaxies.

5.2 Method

We will run models for BCD and dIrr galaxies consisting of gas, stars and dark matter using an N-body/SPH code for the evolution of astrophysical fluids. The model we use was extensively described in previous chapters. Here we summarise the most important features and indicate the parameter choices made. Stars and gas are represented by particles. The stars only experience gravitational forces, calculated using the Barnes-Hut algorithm (Barnes & Hut 1986), whereas the gas particles also experience forces representing gas dynamical forces by use of the smoothed particle hydrodynamics (SPH). To model the interstellar medium we add a model for the neutral gas physics, star formation and for feedback from young stellar clusters.

Model for the interstellar medium

We will use the full model as described in Chapter 2 (“model D”), which is a representation of the neutral phases of the ISM that solves for the thermal and ionization evolution, including cosmic ray ionization and UV heating, including the effects of grain charging. We will run models with a metallicity of $\mathrm{Z} = \mathrm{Z}_\odot/5$, scaled from solar. For the primary ionization rate ζ_{CR} we take $\zeta_{\mathrm{CR}} = 3.6 \times 10^{-17}\ \mathrm{s}^{-1}$.

Star formation recipe

We use the star formation recipe of Gerritsen & Icke (1997). A region is considered unstable to star formation if the local Jeans mass, which for density ρ and sound speed c is given by

$$\mathrm{M_J} = \frac{\pi\rho}{6}\left(\frac{\pi \mathrm{c}^2}{\mathrm{G}\rho}\right)^{3/2}, \qquad (1)$$

is smaller than a reference mass $\mathrm{M_{ref}}$,

$$\mathrm{M_J} < \mathrm{M_{ref}}. \tag{2}$$

The rate of star formation is set to scale with the local free fall time,

$$\tau_{\mathrm{sf}} = \mathrm{f_{sf}} \mathrm{t_{ff}} = \frac{\mathrm{f_{sf}}}{\sqrt{4\pi \mathrm{G}\rho}} \tag{3}$$

The reasoning behind the choice of $\mathrm{M_{ref}}$ and $\mathrm{f_{sf}}$ was described in the discussion of the star formation recipe in Chapter 2. For the models presented here $\mathrm{M_{ref}} = 2 \times 10^5\ \mathrm{M_\odot}$. The delay factor $\mathrm{f_{sf}}$ was chosen to be 2.5. This delay accounts for the fact that the collapse of molecular clouds is inhibited by either turbulence or magnetic fields. Its value is uncertain, and while the dependence of star formation on this parameter was discussed in Gerritsen & Icke (1997), for the models we will present here a subtle issue related to variations in the star formation rate may be raised. Namely, for densities in the order of $\mathrm{n} = 10 - 100\ \mathrm{cm}^-3$, which are the typical densities of star forming particles in our simulation, the free-fall times are in the order of $\tau_{\mathrm{ff}} \approx 5$ Myr. A delay factor $\mathrm{f_{sf}}$ may then suppress variations of the star formation rate on timescales shorter than $\mathrm{f_{sf}}\tau_{\mathrm{ff}}$ Myr. For the simulations presented here we have checked that the results do not differ qualitatively in the range $\mathrm{f_{sf}} = 2.5 - 20$.

The star particles that are formed are assumed to represent stellar associations with a mass distribution formed according to a Salpeter initial mass function (IMF) with a lower mass limit of $0.1\ \mathrm{M_\odot}$ and an upper mass limit of $100\ \mathrm{M_\odot}$.

Feedback from supernova and stellar winds

The feedback method we use is the *pressure particle* feedback method described in chapter 3. This method consists of the creation at the site of a newly formed star particle of a gas-like particle that acts on the surrounding gas as an ordinary SPH particle in the limit of zero mass at constant internal energy. The evolution of the energy of this particle is a model input. We take the following prescription: After an initial time lag $\mathrm{t_l}$ yr, which accounts for the time needed for the heaviest stars of the star cluster to evolve into their terminal phases (thus $\mathrm{t_l} \approx 3 \times 10^6$ yr for an IMF with a $100\ \mathrm{M_\odot}$ upper limit), a constant energy injection rate $\dot{\mathrm{E}}$ is assumed up to the time $\mathrm{t_{sn}}$ at which the last stars of the cluster explode as SN II, hence $\dot{\mathrm{E}} = \epsilon_{\mathrm{sn}} \mathrm{n_{sn}} \mathrm{E_{sn}}/(\mathrm{t_{sn}} - \mathrm{t_l})$, with $\mathrm{E_{sn}} = 10^{51}$ erg the supernova energy, $\epsilon_{\mathrm{sn}} = 0.05 - 0.1$ the efficiency of feedback, $\mathrm{n_{sn}} = 0.009\ \mathrm{M_\odot}^{-1}$ the number of supernovae per solar mass of stars formed and $\mathrm{t_{sn}} = 3 \times 10^7$, the lifetime of an $8\ \mathrm{M_\odot}$ star. The efficiency ϵ_{sn} thus assumes that $90\% - 95\%$ of the original supernova energy is radiated away, a value derived from more detailed simulations of the effect of supernova and stellar winds on the ISM (Silich et al. 1996).

Compared with the simulations presented in Chapter 4 we have added a correction for momentum losses. These losses stem from the fact that we fix the pressure particles to the stellar particle to which it is associated (this is necessary because, carrying no mass, they cannot be assigned an acceleration, see Chapter 3). The effect of this is that the models presented here show somewhat less evolution. Note, however, that hot gas that escapes from the galaxy may in fact carry away angular momentum, and thus the simulations with momentum losses may in fact not be completely unrealistic.

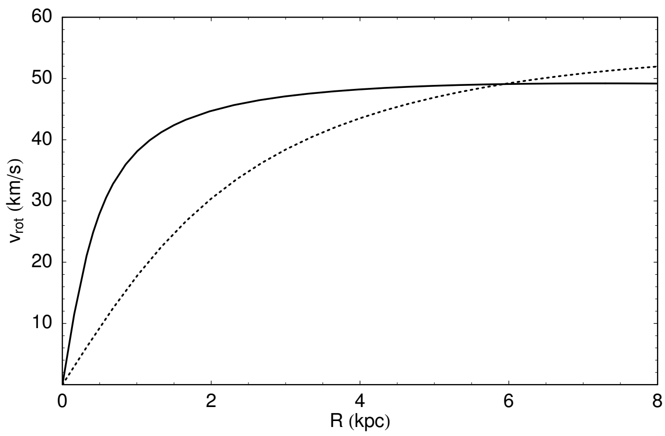

Figure 5.1: Dark halo rotation curves. **Drawn line:** model A, **dotted line:** model B.

5.3 Initial conditions

As we have discussed in the introduction, the central halo density and the angular momentum of the gas disk seem to be the parameters that determine whether a given dIrr galaxy will exhibit BCD features. We will examine the role of these parameters by running models with different halo and gas distributions, chosen to be representative of either BCD or dIrr. Other parameters like the masses of the gaseous, stellar and dark components, will be kept the same.

We will run simulations for dwarf galaxies in isolation. Note that the environment of dwarf galaxies may have a strong effect on their evolution, and indeed environment has been shown to correlate with galaxy type, with early type dwarfs showing a preference for dense cluster environments (Binggeli et al. 1990). Ram pressure stripping, tidal interactions and collisions with HI clouds all may act to perturb the ISM of dwarf galaxies and lead to enhancements of the SFR, or, in drastic cases, total removal of the ISM. Also note that interactions may very well change the distribution of angular momentum and thus affect the gas distribution or dark matter distribution; these are separate sources of evolution we will not consider (see e.g. Marcolini et al. 2003, Mori & Burkert 2000 and Mayer et al. 2001, Pasetto et al. 2003 for recent work on these).

Meurer et al. (1998) noted that the halo densities for the BCD NGC 1705 and 2915 are in the range $0.1 - 0.3$, a factor 10 higher than for normal dIrr. This is also consistent with the steeply rising rotation curves of BCDs found by other people (e.g. van Zee et al. 2001), as these imply high halo densities if these BCDs are dominated at all radii by the dark halo (as is probably the case). Thus we will consider two different halo models: one sharply peaked BCD-like, designated with A, and one with a large constant density core typical for dIrr, designated B. Both models will be chosen such that the rotation velocity of the halo is about the same at a radius of 6 kpc. To be specific, we take a density profile

$$\rho_{\rm h}({\rm r}) = \rho_0 \frac{\exp(-{\rm r}^2/{\rm r}_{\rm c}^2)}{1 + {\rm r}^2/\gamma^2}. \qquad (4)$$

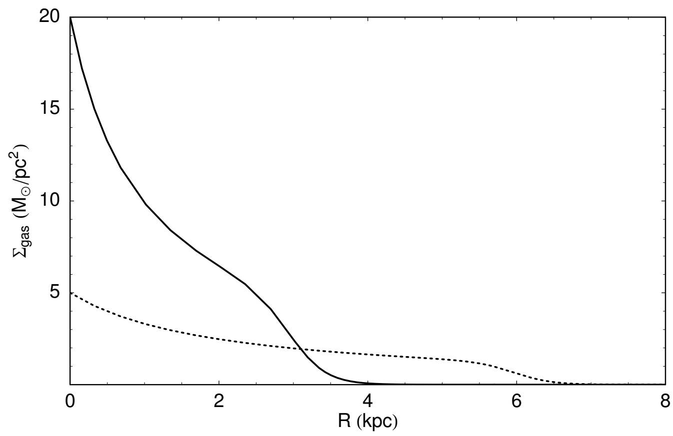

Figure 5.2: Gas surface density of the galaxy models. **drawn line:** model 1, **dotted line:** model 2. Both models have the same total mass.

For the model A we take a central halo density $\rho_0 = 0.32\ \mathrm{M_\odot/pc^3}$ and a core radius $\gamma = 0.4$ kpc, while for model B we take $\rho_0 = 0.02\ \mathrm{M_\odot/pc^3}$ and $\gamma = 2$ kpc. In both cases the cutoff radius $\mathrm{r_c}$ is taken to be $\mathrm{r_c} = 20$ kpc. The halos are represented by static potentials. A plot of the resulting halo rotation curves is given in Fig. 5.1.

An indication of the typical range of central gas surface densities for BCDs and dIrr can be found in van Zee et al. (2001). In their Figure 10 a sample of BCDs has its gas density profile compared to a dIrr sample. BCDs shown there have central densities in the order of $20\ \mathrm{M_\odot/pc^2}$, where dIrr show lower surface densities, in the range $3 - 10\mathrm{M_\odot/pc^2}$. For the gas disk we take then the following parametrization of the surface density,

$$\Sigma = \frac{\Sigma_\mathrm{g}}{1 + \mathrm{R/R_g}} \frac{1}{1 + \mathrm{e}^{(\mathrm{r-R_t})/\Delta\mathrm{R_t}}}, \qquad (5)$$

where we will examine two different models, both with a mass of about $\mathrm{M_{gas}} = 2 \times 10^8\ \mathrm{M_\odot}$, with gas disk 1 having radial scale $\mathrm{R_g} = 0.98$ kpc, central surface density $\Sigma_\mathrm{g} = 20\ \mathrm{M_\odot/pc^2}$ and a truncation radius at $\mathrm{R_t} = 3$ kpc, while disk 2 has $\mathrm{R_g} = 1.96$ kpc, $\Sigma_\mathrm{g} = 5\ \mathrm{M_\odot/pc^2}$ and $\mathrm{R_t} = 6$ kpc. In both cases $\Delta\mathrm{R_t} = 0.25$ kpc. The two gas distributions are plotted in Fig. 5.2.

Combining halo and gas disk we get a 2×2 grid of models A1, A2, B1 and B2. the A1 model resembles an archetypical BCD, while "normal" dIrrs are more like model B2. The two other models A2 and B1 are of mixed type and serve to disentangle the effect of the halo parameters from that of the gas distribution (but note that these models are not less realistic, because in principle the gaseous and dark components can undergo wholly different evolution).

The initial stellar distribution is taken the same for all models, namely an exponential disk with a sech-squared z distribution,

$$\rho_\mathrm{disk}(\mathrm{R,z}) = \frac{\Sigma_0}{2\mathrm{h_z}} \exp(-\mathrm{R/R_d})\mathrm{sech}^2(\mathrm{z/h_z}) \qquad (6)$$

with central surface density $\Sigma_0 = 200\ \mathrm{M_\odot/pc^2}$, a radial scale length $\mathrm{R_d} = 0.6$ kpc and a vertical scale height $\mathrm{h_z} = 250$ pc. It is constructed using the method described in

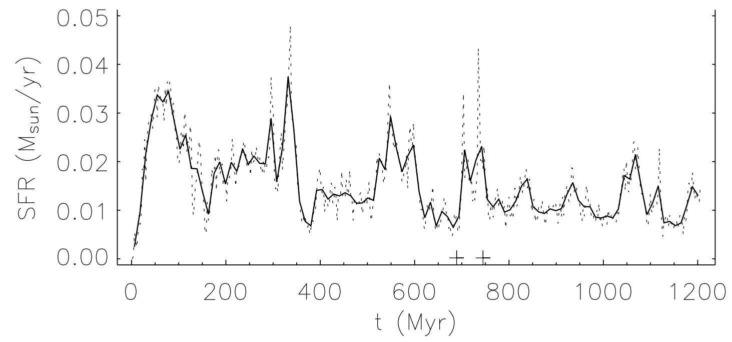

Figure 5.3: Total star formation rate of model A1. Drawn line indicates the SFR determined by binning star formation events in 10 Myr intervals, dotted line is the same for 2 Myr bins. Crosses indicate the times for which the snapshots shown in Fig. 5.8 are taken.

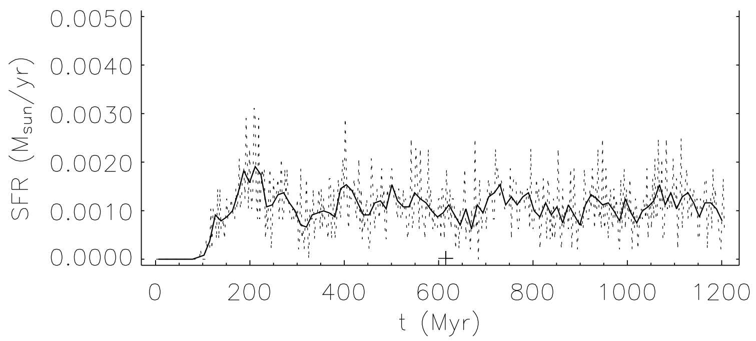

Figure 5.4: Total star formation rate of model B2. Drawn line indicates the SFR determined by binning star formation events in 10 Myr intervals, dotted line is the same for 2 Myr bins. The cross is the time of the snapshot shown in Fig.5.10.

Kuijken & Dubinski (1995), calculating an approximate 3 integral distribution function accounting for the halo and gas potentials. The total mass of the stellar disk is $\mathrm{M_d} = 10^8\ \mathrm{M_\odot}$. The initial ages of the stars are distributed according a star formation rate of $0.008\ \mathrm{M_\odot}$/yr

The simulations shown here are run with 50k gas particles and 50k star particles. We take some care in preparing the gas disks, especially for the A1 and B1 model. As these models can show disruptive bursts of star formation (up to $0.1 - 0.2\ \mathrm{M_\odot}$/yr) if the initial particle dispersion is chosen too low (lower than about 10 km/s).

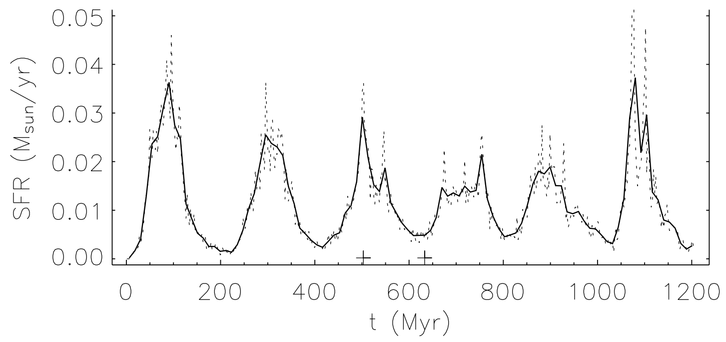

Figure 5.5: Star formation rate of model B1. Drawn line indicates the SFR determined by binning star formation events in 10 Myr intervals, dotted line is the same for 2 Myr bins. Crosses indicate the times for which the snapshots shown in Fig. 5.9 are taken.

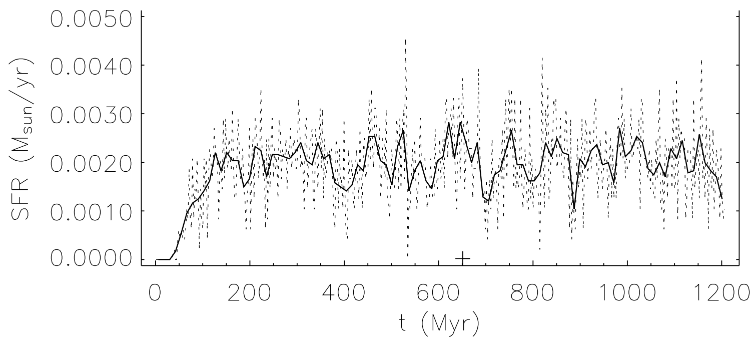

Figure 5.6: Total star formation rate of model B2. Drawn line indicates the SFR determined by binning star formation events in 10 Myr intervals, dotted line is the same for 2 Myr bins. The cross is the time of the snapshot shown in Fig.5.10.

5.4 Results

We run the simulations for about 1500 Myr, which is long enough for a quasi steady state to develop, but short enough so that the effects of sources of evolution not included in the model (e.g. enrichment, gas infall or interaction) can be ignored.

In Fig. 5.3 and 5.4 we have plotted the resulting star formation rate of the "pure" BCD model A1 and the dIrr model B2. We see that, while the total gas content is equal, the two models show drastically different star formation properties. The A1 model has a typical star formation rate of about $0.015\ \mathrm{M}_{\odot}$/yr, with sizable excursions up to $0.05\ \mathrm{M}_{\odot}$/yr, while the B2 model has a much lower star formation rate, $\approx 0.001\ \mathrm{M}_{\odot}$/yr, with also much smaller variations. The variations that are visible are for a large part statistical variations due to the finite size of the star particles that are formed.

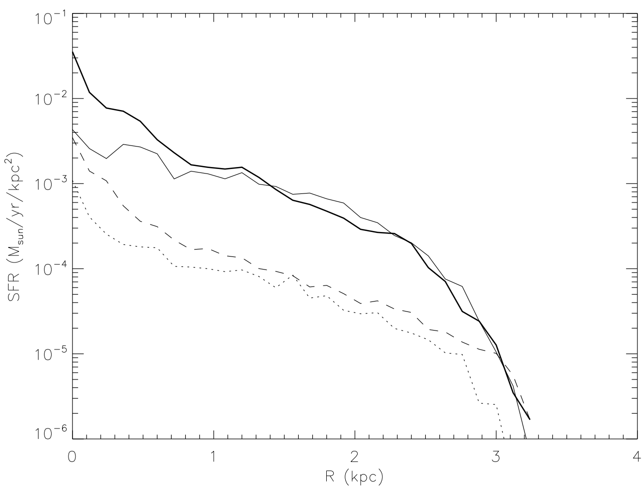

Figure 5.7: Mean star formation density as a function of radius. **Thick line:** A1 model, **thin line:** B1 model, **dashed:** A2 model and **dotted:** B2 model.

If we look at the star formation rate of the B1 and A2 models (Fig. 5.5 and 5.6), we again see the same big difference in star formation rate for the high surface density and low surface density models. The star formation rate of the low surface density model (A2) shows little variations, being very similar to the B2 model, although slightly higher with a $\mathrm{SFR} \approx 0.002$. On the other hand, while for the A1 and B1 model the SFR are about the same, we see that the variations in star formation rate follow a much more regular pattern in the case of B1 model. This is due to the large constant density core of this model (see also the discussion in chapter 4).

More information about the spatial distribution of star formation is given by Fig. 5.7, where the time averaged star formation density is plotted as a function of radius. A number of observations can be made on the basis of this picture. First, if we look at the differences between the A1 model and B1 model we see that, while the star formation rate per unit area is about the same at the outskirts, in the center it is about a factor of 10 higher for the A1 model. This difference does not translate into a big difference in the overall (mean) star formation rate. The A2 and B2 models have lower star formation densities than the models with a concentrated gas distribution, but otherwise a very similar dependence on radius. The star formation of the model run with halo A again peaks higher than the B halo. We see that the star formation rate is mainly set by the gas (surface) density (as expected). A denser halo will enhance the star formation in the central region.

Note that for all models the star formation drops at a radius of about 3 kpc. To some extent this is a coincidence because the threshold radius can be shifted by changing the cosmic ray heating (see Chapter 2). For higher cosmic ray fluxes star formation will be confined to a smaller region. However, 3 kpc is also close to the radius at which the stellar disk is terminated. This may point to a connection of star formation with previous existing stellar populations. This is supported by the fact that the

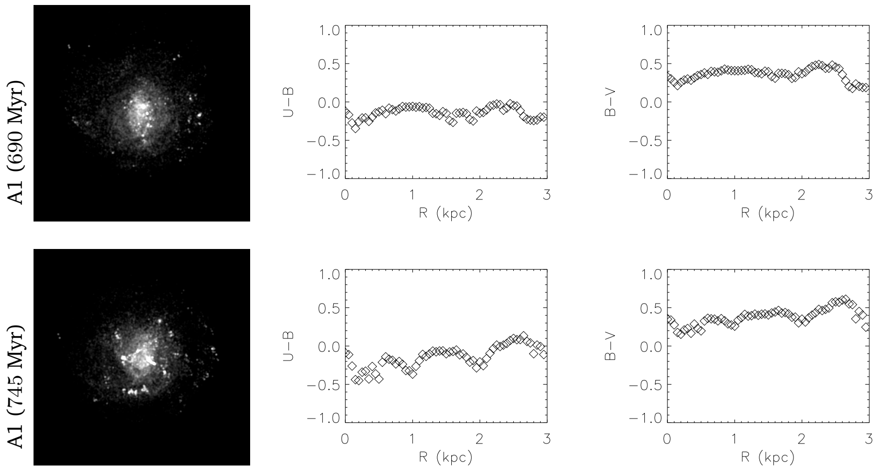

Figure 5.8: Optical properties of model A1. UBV composites (see appendix for colour) and plots of U − B and B − V colours at simulation times of 690 Myr (upper panels) and 745 Myr (lower panels).

scale height of the gas disk as function of radius shows a kink where the stellar disks terminates.

5.5 Observational properties of simulated galaxies

From the stellar distributions, the ages of the stellar particles and the Bruzual & Charlot (1993) population synthesis tables we construct U, B and V maps. In Fig. 5.8 we have plotted for the A1 simulation UBV composites as well as the radial dependence of the U − B and B − V colours. These are shown for two representative frames, chosen to be at a time of relatively low star formation (at a simulation time of 690 Myr) and the other at a time of increased star formation (745 Myr). If we compare the UBV composites with analogous maps for the B1 simulation (Fig. 5.9) and the A2 and B2 models (Fig. 5.10) we see that the A1 snapshots show a strong centrally concentrated light distribution, whereas the B1 model shows more widely distributed patches of star formation. The A2 and B2 composites show little features.

The colours of dIrr and BCD galaxies are generally quite blue (with $\mathrm{U} - \mathrm{B} \lesssim -0.1$ and $\mathrm{B} - \mathrm{V} \lesssim 0.5$). Comparing BCD with dIrr, the former have less colour gradients than the latter, with BCDs having positive radial U − B and B − V gradients, and thus reddening on the outside. The azimuthally averaged colour plots from the simulated U, B and V maps shown in Figures 5.8, 5.9 and 5.10 should be seen as rough approximations only. We do not take into account extinction. Furthermore, the initial stellar population is taken to be the same for all simulations. This means the colours are not realistic, because the colours depend on the total star formation history. Nevertheless we can look at general trend and compare the different models. We see that the A1 and B1 models are much bluer than the A2 and B2 model, this is due to the initial stellar population (too much old stars are present for the A2 and

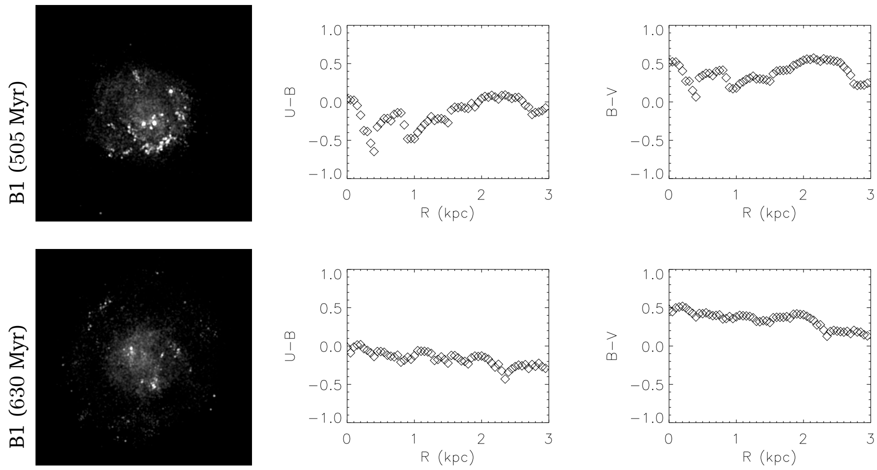

Figure 5.9: Optical properties of model B1. UBV composites and plots of U − B and B − V colours at simulation times of 690 Myr (upper panels) and 745 Myr (lower panels).

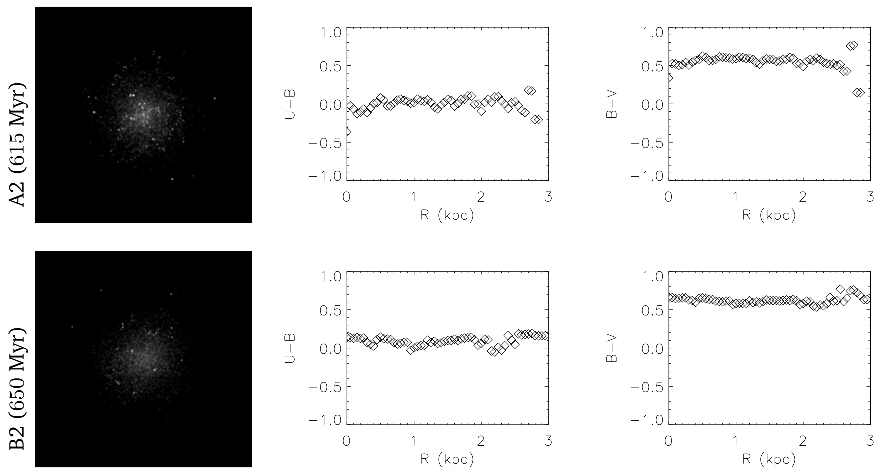

Figure 5.10: Optical properties of models A2 (upper panels) and B2 (lower panels). UBV composites and plots of U − B and B − V colours.

B2 models in relation to their current star formation). If we look at the radial colour distribution we see that the A1 models show either no colour gradient or reddening from the inside to the outside, whereas the B1 model shows little trend or a negative colour gradient. The A2 and B2 show no colour gradients.

5.6 Discussion and conclusions

If we would classify our galaxies on the basis of the optical characteristics given in Figures 5.8, 5.9 and 5.10, the A1 model would be a good BCD candidate, the B2 model a vigorously star forming dIrr and B2 and A2 model would represent low surface brightness dwarfs. The A1 model has many of the the characteristics associated with the BCD phenomenon: central star formation, compact optical scale lengths, reddening with increasing radius. That such a system is the outcome of a model galaxy made according to the characteristic halo and gas distribution of observed BCDs is confirmation that these properties are indeed the determining factors for the BCD mode of star formation. Note that we have shown that both a compact gas distribution *and* a centrally concentrated halo are necessary. A high gas surface density will imply a high star formation rate, but the central concentration is a result of the high halo density. This does not mean that dIrr with a low central halo density could not experience a central bursts of star formation (and thus maybe classified as BCDs), but only that on the basis of our simulations we expect such a burst to be a transient 'false' BCD phase. On the other hand, we have not found that the A1 model undergoes phases of low star formation: it seems to stay in a BCD mode, essentially until the gas reservoir is (locally) depleted.

Our low surface density simulations (A2 and B2) show low star formation, regardless of halo density. We do not expect dIrrs with low gas densities to undergo large star formation bursts, unless perturbed by some external effect.

There are some areas that still need to be explored. One is the effect of a halo built from particles as opposed to a halo consisting of a static potential. Such a halo can react dynamically on perturbations. The other is role the metallicity. We chose a metallicity of $Z = Z_{\odot}/5$, which is realistic for both normal dIrr and BCDs, although a bit on the high side for BCDs. A lower metallicity may have an effect on star formation. Also, our simulation does not answer the question why the BCDs should have lower metallicity. It could be that BCDs have had too little time for enrichment. The fact that our simulations imply that the BCD phase persists until gas depletion automatically implies that current BCDs can only be a few Gyr old, younger than dIrr. This would be consistent with the presence of BCD systems that are proven to be very young (less than 1 Gyr, Izotov & Thuan 2004). "Old" BCDs, meaning systems that have "turned" on more than a few Gyrs ago, would then have evolved, due to gas depletion into the general dIrr population, changing into a more leisurely mode of star formation or they may have turned into dEs. In the process they could lose their centrally condensed halo due to mass loss effects (Navarro & White 1993). It is interesting to note that BCD-like systems are thought to constitute the building blocks of galaxies at high redshifts. It may that the current population of BCDs are just a trickle of late galaxy formation, and that they are relics of a bygone era.

References

Barnes, J. & Hut, P., 1986, *Nature* **324**, 446

Binggeli, B., Tarenghi, M., & Sandage, A., 1990, *A&A* **228**, 42

Bruzual A., G. & Charlot, S., 1993, *ApJ* **405**, 538

Gerritsen, J. P. E. & Icke, V., 1997, *A&A* **325**, 972
Hunter, D. A. & Elmegreen, B. G., 2004, *AJ* **128**, 2170
Hunter, D. A., Elmegreen, B. G., & Baker, A. L., 1998, *ApJ* **493**, 595
Izotov, Y. I. & Thuan, T. X., 2004, *ApJ* **616**, 768
Kennicutt, R. C., 1989, *ApJ* **344**, 685
Kuijken, K. & Dubinski, J., 1995, *MNRAS* **277**, 1341
Marcolini, A., Brighenti, F., & D'Ercole, A., 2003, *MNRAS* **345**, 1329
Mayer, L., Governato, F., Colpi, M., Moore, B., Quinn, T., Wadsley, J., Stadel, J., & Lake, G., 2001, *ApJ* **559**, 754
Meurer, G. R., Staveley-Smith, L., & Killeen, N. E. B., 1998, *MNRAS* **300**, 705
Mori, M. & Burkert, A., 2000, *ApJ* **538**, 559
Navarro, J. F. & White, S. D. M., 1993, *MNRAS* **265**, 271
Papaderos, P., Loose, H.-H., Thuan, T. X., & Fricke, K. J., 1996, *A&AS* **120**, 207
Pasetto, S., Chiosi, C., & Carraro, G., 2003, *A&A* **405**, 931
Schmidt, M., 1959, *ApJ* **129**, 243
Silich, S. A., Franco, J., Palous, J., & Tenorio-Tagle, G., 1996, *ApJ* **468**, 722
Thuan, T. X. & Martin, G. E., 1981, *ApJ* **247**, 823
van Zee, L., 2001, *AJ* **121**, 2003
van Zee, L., Salzer, J. J., & Skillman, E. D., 2001, *AJ* **122**, 121
van Zee, L., Skillman, E. D., & Salzer, J. J., 1998, *AJ* **116**, 1186